molecular pharmaceutics

pubs.acs.org/molecularpharmaceutics

Article

Integrative Salt Selection and Formulation Optimization: Perspectives of Disproportionation and Microenvironmental pH Modulation

Shikhar Mohan, Yi Li, Kevin Chu, Liliana De La Paz, Diana Sperger, Bing Shi, Chris Foti, Victor Rucker, and Chiajen Lai*

Cite This: *Mol. Pharmaceutics* 2024, 21, 2590−2605

Read Online

ACCESS | Metrics & More | Article Recommendations

ABSTRACT: We report a novel utilization of a pH modifier as a disproportionation retardant in a tablet formulation. The drug molecule of interest has significant bioavailability challenges that require solubility enhancement. In addition to limited salt/cocrystal options, disproportionation of the potential salt(s) was identified as a substantial risk. Using a combination of Raman spectroscopy with chemometrics and quantitative X-ray diffraction in specially designed stress testing, we investigated the disproportionation phenomena. The learnings and insight drawn from crystallography drove the selection of the maleate form as the target API. Inspired by the fumarate form's unique stability and solubility characteristics, we used fumaric acid as the microenvironmental pH modulator. Proof-of-concept experiments with high-risk (HCl) and moderate-risk (maleate) scenarios confirmed the synergistic advantage of fumaric acid, which interacts with the freebase released by disproportionation to form a more soluble species. The resultant hemifumarate helps maintain the solubility at an elevated level. This work demonstrates an innovative technique to mediate the solubility drop during the "parachute" phase of drug absorption using compendial excipients, and this approach can potentially serve as an effective risk-mitigating strategy for salt disproportionation.

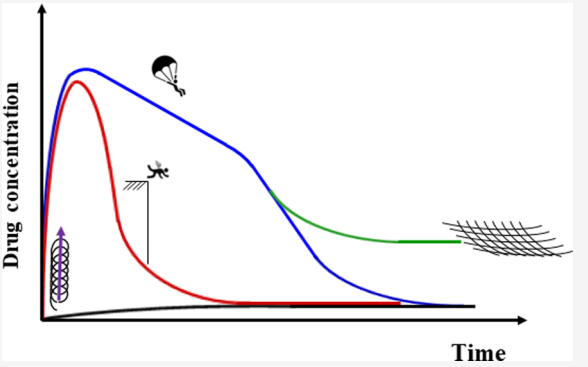

KEYWORDS: *Raman spectroscopy, X-ray diffraction, chemometrics, microenvironmental pH, salt disproportionation, formulation, pH modifier, spring-and-parachute*

1. INTRODUCTION

The increasing structural complexity and molecular weight of new drug molecules come with significant hurdles for product development, specifically the solubility and dissolution properties. Approximately 40% of marketed drugs and a majority (>70%) of new molecular entities (NME) are categorized as BCS class II or class IV compounds with poor solubility that lead to low or erratic bioavailability.[1,2] Researchers apply various formulation technologies to overcome challenges resulting from low solubilities and unpredictable dissolution.[3] These approaches include micronization, nanosuspension,[4] cyclodextrin complexation,[5] or amorphous solid dispersions.[6,7] If the drug molecule has an ionizable group, forming a salt is the most straightforward and cost-effective strategy for solubility enhancement due to the ease of integration into API synthesis and drug product manufacturing. Additionally, under the FDA directive that drugs containing cocrystals are considered new polymorphs of the API,[8] cocrystal formation also creates a new dimension of opportunities in the drug delivery, regulatory, and intellectual property landscape.[9]

Despite the apparent simplicity, choosing salt as the pharmaceutical product is a convoluted exercise that requires thorough assessments and continuous optimization. Most drug molecules are weak electrolytes (acids or bases). If the pK_a differential (ΔpK_a) is greater than 2,[10−12] the acid−base reaction is chemically possible. However, the salt formation does not necessarily lead to crystalline solids with suitable physical characteristics (e.g., stability, hygroscopicity). Depending on the dosage, researchers could be further constrained by the toxicity and permissible daily exposure (PDE) of acid or base coformers.[13,14] These considerations usually translate to a limited set of counterion options for the drug substance.

Received: February 14, 2024
Revised: April 11, 2024
Accepted: April 12, 2024
Published: April 24, 2024

https://doi.org/10.1021/acs.molpharmaceut.4c00166
Mol. Pharmaceutics 2024, 21, 2590−2605

The most critical liability of using salts as the API is their propensity of disproportionation, where the ionized species (salt) reverts to the neutral molecule due to pH changes encountered in the gastrointestinal tract.[15−18] Disproportionation may compromise the formulation performance and defeat the purpose of using salt as the product. The negative impact is often manifested in the form of decreased dissolution and reduced bioavailability, both of which add to the development burden to further optimize the formulation.[19]

There is a wealth of information in the literature on the investigations of disproportionation from various aspects: the mechanism, quantitation, and minimization strategy. Factors influencing disproportionation can be generally divided into two categories: variables related to salt properties, and variables related to excipients, formulation design, and manufacturing processes.

The first group of factors are inherent to the salt itself, specifically its solubility behavior and pH_{max}.[10,15,18,20,21] In the pH-solubility profile of a molecule, pH_{max} is the pH where the salt and the neutral species are in equilibrium, representing the maximum total solubility in the solution.[22,23] For a weak base API, pH_{max} can be expressed as[20,22,24]

$$pH_{max} = pK_a + \log\frac{S_{FB}}{S_{salt}} \quad (1)$$

Or alternatively

$$pH_{max} = pK_a + \log\frac{S_{FB}}{\sqrt{K_{SP}}} \quad (2)$$

where pK_a is the acid dissociation constant for the base, S_{FB} is the solubility of the freebase, S_{salt} is the solubility of the salt, and K_{sp} is the solubility product of the salt.

Similar equations for weak acid APIs can be found in the literature.[10,18]

The thermodynamic driving force for disproportionation (salt → neutral) can be estimated by the Gibbs free energy difference,[16] i.e.

$$\Delta G \approx -RT \ln K_a\left[\frac{S_{salt}^2}{S_{FB}}\right] \quad (3)$$

Therefore, a high solubility difference leads to a higher risk of disproportionation. For weak base API where the solubility increases dramatically with decreasing pH, a higher pH_{max} is more desirable. Molecules are completely ionized (in salt form) at pH < pH_{max}. Thus, a higher pH_{max} corresponds to a broader pH range of high solubility. The implication of eqs 1 and 2 is that a higher pK_a and freebase solubility with a lower salt solubility would disfavor disproportionation for a weak base API.

Merritt et al.[20] have proposed a mathematical framework to analyze disproportionation propensity. Their mechanistic model, verified by a diverse set of compounds, greatly enhanced researchers' ability to gauge the risk in early-phase development with simple lab measurements. There are studies investigating other minor effects, such as API particle size[17] or counterion buffering capacity.[18] However, the pH_{max} values (counterion specific), the implications from eqs 1−3, and the limited number of salts considered safe for administration in humans are usually the primary factors guiding the salt selection.

The second group of factors that influence disproportionation is the excipients, the chemical environment created by the excipients, and processing or storage conditions such as temperature,[23,25] relative humidity,[21,23] or mechanical stress during manufacturing.[23,25] This broad range of factors is part of the grand scheme of the formulation design. The selection of excipients is of paramount importance because disproportionation often takes place through an excipient-induced solution-mediated mechanism.[23] Among the excipient properties, its acidity/basicity,[23,25,26] aqueous solubility,[15] buffering capacity,[15,18,21] structural integrity (amorphous/crystalline, particle size/surface area),[15,18,25] and hygroscopicity/water activity[21,25] are all important parameters. Numerous studies have covered these aspects, including alternative approaches such as using polymer matrices to minimize API/excipient contacts.[27] Since each dosage form is unique, formulation optimization often reflects the balance of benefits and risks rather than a single, fixed recipe.

Two crucial concepts stemming from the discussion above are pH-dependent solubility and microenvironmental pH. Whether the API is in the neutral form or a salt, pH-dependent solubility or uncontrolled disproportionation could be detrimental to the performance of the drug. One of the main objectives of formulation development is to achieve pH-independent dissolution, for the drug to weather through the pH swings in the gastrointestinal tract and deliver the intended dosage at the right place and time. Thus, manipulating pH-solubility through formulation has been the focus of research, not only for dissolution but sometimes for stability's sake as well.[28−30] A plethora of pH-modulation approaches are available, mostly applicable to both crystalline APIs[28,31−33] and amorphous dispersions.[29,34−36]

Microenvironmental pH (denoted as pH_M) is defined as the pH of the saturated solution in the immediate vicinity of the surrounding drug particles.[37,38] It was recognized through decades of research that the diffusion layer is critical to the dynamics of the dissolution process.[39,40] The Noyes−Whitney equation defines the drug dissolution rate as[33,41]

$$\frac{dC_b}{dt} = \frac{DS}{Vh}(C_s - C_b) \quad (4)$$

where t is the time, D is the diffusion coefficient, V is the volume, h is the thickness of the diffusion layer, C_b is the drug concentration in the bulk medium, and C_s the drug's solubility near the solid interface. Manipulating the localized condition (i.e., the microenvironment) of C_s would be the most efficient and realistic path to enhance the dissolution of the drug.

Among the pH-modulation approaches, adding a pH modifier as an excipient is the most common strategy to achieve pH-independent solubility. There are examples of using enteric polymer or carriers to optimize the release further;[26,30,31] however, most of the cases have been the addition of small-molecule acids or bases, particularly organic acids (e.g., citric, succinic, tartaric)[31−33,38] or alkalizers (e.g., sodium carbonates, magnesium oxide).[28−30,34,35,42] A summary of the physical properties of these frequently used pH modifiers can be found in the literature.[34] The pH modifiers' effectiveness in controlling microenvironmental pH (pH_M) varies with their acid/base strength (pK_a) and aqueous solubility. While extensive research focused on the rank-ordering of different acids or bases,[29,32,35,43] the comparisons are often drug-specific and further complicated by secondary factors such as microscopic vs macroscopic mixing.[29] To

https://doi.org/10.1021/acs.molpharmaceut.4c00166
Mol. Pharmaceutics 2024, 21, 2590−2605

enable better absorption in vivo, an ideal pH modifier should modulate the pH to be near the pH_{max} and maintain the condition for an extended duration. This optimal scenario usually occurs when the pH modifier's release rate is comparable to or slightly slower than the drug release rate during the dissolution process.[34]

The study described herein provides a case for the formulation optimization of a development compound. From the product performance perspective, an API salt was required due to the freebase's impractically low solubility. However, only 3 crystalline salts/cocrystals of the API were found after extensive screening of acid coformers from the generally recognized as safe (GRAS) and class 1 and 2 lists.[14] We approach the selection and the subsequent optimization in an unconventional way: by assessing the disproportionation risks of the identified API salts. Achieving high solubility through salt formation was desirable; however, minimizing disproportionation, the most intrinsic risk associated with an API salt, was equally important. In the context of the spring-and-parachute model,[44,45] consistent and satisfactory bioavailability can only be achieved for a poorly soluble drug when the "parachute" phase of the drug release can be predicted and controlled. We leveraged the insight from crystallography and chemometrics to thoroughly investigate disproportionation (kinetics and quantitation) as a differentiation factor to enable salt selection. The learning has greatly benefited the formulation development. While many industrial precedents focused on the use of polymer (especially for formulations involving amorphous solid dispersions)[46] as a crystallization inhibitor to prevent the neutral form precipitation, we used a cocrystal former (fumaric acid) that serves dual purposes: (1) microenvironmental pH-modulation (pH_M) and (2) formation of a favorable cocrystal that eliminates the freebase produced by disproportionation. The resulting formulation allowed us to achieve target bioavailability by using compendial ingredients in a synergistic way.

2. EXPERIMENTAL SECTION

2.1. Materials. Compound X is an API molecule under development. Its chemical structure and properties have been reported as API 2 in a recent publication.[47] The neutral form of the molecule (a weak base) is known to exist in many polymorphs (Forms I, II, III, IV, V),[48] all solvent-free with distinct melting points. Despite being early in development, the synthetic route has consistently produced high-purity (>99.5%) drug substances for pharmaceutical development.

The API freebase formed crystalline salts/cocrystals with a selective list of counterions, all procured from the Aldrich Company (Aldrich, OH) and used directly without further purification. Chromatography-grade water was used as the only solvent for the disproportionation studies.

2.2. Equipment. *2.2.1. Reactor Setup.* Crystallization and disproportionation experiments were performed in a 100 mL glass reactor (EasyMax 402, with an isothermal stand for a 100 mL vessel, Mettler Toledo). A 38 mm diameter overhead agitator and a pitched-blade element with a 45° angle to enable downward flow were used as the primary mechanism of mixing. An in-line Raman probe (Kaiser Optical Systems, Inc.) and an FBRM probe (Focused Beam Reflectance Measurement, Mettler Toledo) were used for process monitoring. For consistency, the Raman and FBRM probes were placed in the same position throughout the investigation to ensure the system's hydrodynamics (mechanical shear) do not introduce batch-to-batch variation of disproportionation. The reactor configuration (along with PAT probes) is shown in Figure 1.

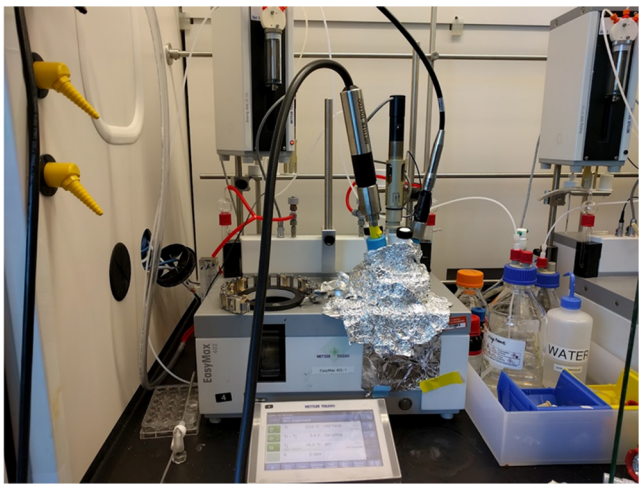

Figure 1. Reactor setup for the salt disproportionation study.

2.2.2. Raman Spectroscopy. Raman data was recorded using a RamanRxn2 Analyzer (Kaiser Optical Systems, Inc.) equipped with a fiber-optic probe, using 250 mW, 785 nm laser excitation. The observable spectral range of this system was from 100 to 3425 cm^{-1} with a resolution of 1 cm^{-1}. The acquisition conditions have been optimized; each spectrum has an exposure time of 60 s, with 60 s of pause between acquisitions. The batch was kept from room light to minimize fluorescence interference with the Raman spectra. The icRaman software (Build 4.4.21, Mettler Toledo) was the user interface for instrument configuration and data acquisition. Chemometric modeling, spectral preprocessing, and analyses were performed through MATLAB (version R2019b, Mathworks, Inc., MA) and PLS_Toolbox (version 821, Eigenvector Research, Inc., WA).

2.2.3. X-ray Diffraction. X-ray diffraction patterns were collected with a PANalytical X'Pert PRO MPD diffractometer using an incident beam of copper (Cu Kα, λ = 1.5418 Å) radiation produced using a long, fine-focus source and a nickel filter. The diffractometer was configured using a symmetric Bragg−Brentano geometry. Before the analysis, a silicon specimen (NIST SRM 640e) was analyzed to verify that the observed position of the Si 111 peak was consistent with the NIST-certified position. Samples were prepared for analysis by packing the powder sample in the center of a cavity (10 mm diameter) within a silicone zero-background substrate. Soller slits for the incident and diffracted beams were used to minimize broadening from axial divergence. Diffraction patterns were collected using a scanning position-sensitive detector (X'Celerator) located at 240 mm from the sample. The X-ray generator was operated at a voltage of 45 kV and amperage of 40 mA. The sample rotation during measurement was kept at 2 revolutions/second. Scans were performed from 2 to 40° 2θ range. The step size was 0.008°, and the total scan time was 1 h. Diffraction data was analyzed by X'Pert Highscore version 2.2c (PANalytical B.V., Almelo, Netherlands) and X'Pert data viewer version 1.9a.

2.3. Methods. *2.3.1. X-ray Quantitation and Calibration.* During disproportionation experiments, the API salt reverts to one or more API freebase forms. In those circumstances, the

https://doi.org/10.1021/acs.molpharmaceut.4c00166
Mol. Pharmaceutics 2024, 21, 2590−2605

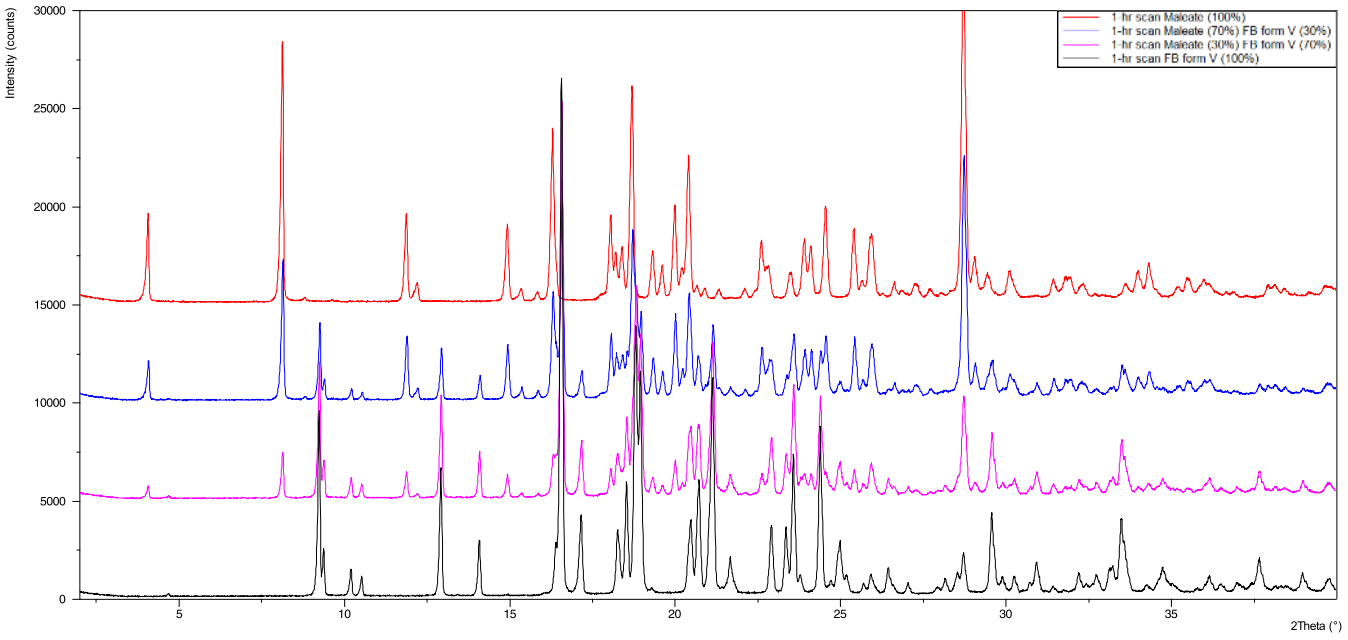

Figure 2. X-ray overlay of physical mixtures of maleate and freebase Form V at selective compositions.

slurry contains the original salt and multiple freebase forms, making form quantitation a significant analytical challenge. Our approach was to use binary calibrations as the basis of quantitation. The use of X-ray peak intensity (height or area) ratios to determine phase composition is a widely accepted practice.[49,50] For binary mixtures, we use integrated peak area, as it is less sensitive to background noise and algorithm selection compared to the peak height approach. For example, physical mixtures of maleate and freebase Form V were made in 10% increments and slurried in an inert solvent (e.g., cyclohexane). Solid was thoroughly mixed by vortex mixing and isolated by centrifuge filtration. The mixture samples were subject to X-ray analyses with 1 h scans. Figure 2 shows the X-ray overlay of pure maleate (top), pure freebase form V (bottom), and two representative mixtures at 30 and 70% (w/w) compositions. Four calibrations with different peak combinations (peaks characteristic of each pure form) are shown in Figure 3. Multiple calibrations were used to ensure method robustness, as preferred orientation from specific morphology (e.g., needles) could lead to an out-of-proportion peak size in certain situations.

2.3.2. Raman Quantitation and Calibration. The disproportionation process was monitored at various concentrations of the salts. A quantitative model was generated for each combination of concentration and counterion, resulting in a total of eight models (two counterions, each measured at four slurry concentrations). The model was developed by collecting a set of approximately 5−8 Raman spectra and offline X-ray diffractograms representing the entire duration of the disproportionation process. The offline quantitation by X-ray was used as a reference for the Raman spectra collected at the corresponding time. A partial least-squares (PLS) model was generated between the preprocessed Raman spectra and X-ray quantitative results. The preprocessing included truncation of the spectral range to emphasize form-indicating regions and mean-centering to comply with the PLS algorithm. The developed models were evaluated by cross-validation via Venetian blind with 10 splits. The resulting root-mean-square error of cross-validation (RMSECV) was used to compare model accuracy.

2.3.3. Disproportionation Process Description. Disproportionation kinetics were examined with the reactor setup shown in Figure 1. The experimental procedure varied depending on the parameters being evaluated; however, the general procedure was as follows:

- Charge 100 mL of HPLC-grade water into the EasyMax vessel.
- Preheat the water to 50 °C (batch temperature) with agitation at 500 rpm. Throughout the experiment, the temperature and agitation were maintained constant.
- Start Raman and FBRM data acquisition.
- Charge an appropriate amount of salts (e.g., maleate, HCl salt) and (optionally) additives (e.g., fumaric acid, tartaric acid) to the reactor (t = 0) and monitor the disproportionation process.
- Periodically obtain aliquot samples for offline X-ray analyses.
- Isolate the slurry at the end of the experiment. Measure supernatant pH and collect solid product for polymorph quantitation.

Experimental conditions were selected to cover four volume/weight (solvent/salt in mL/g) ratios: 20, 40, 60, and 80. The corresponding slurry concentrations are 50, 25, 16.7, and 12.5 mg/mL, respectively. Lower concentrations were not evaluated due to poor signal-to-noise ratio in Raman spectra and insufficient solids for X-ray analysis from slurry samples.

2.3.4. Intrinsic Dissolution Rate. The intrinsic dissolution rate (IDR) of various forms was determined using a USP Type 2 dissolution apparatus in 900 mL of 0.01 N hydrochloric acid (pH 2.0) or 20 mM phosphate buffer (pH 6.8). IDR measurements were performed at a constant temperature of 37 °C and a disk rotation speed of 100 rpm. Disks were prepared by directly compressing approximately 100 mg of API powder in a die using a hydraulic press (Carver Press, Fred Carver, NJ) to form a smooth surfaced pellet. Liquid samples from the dissolution medium were analyzed by ultra-

https://doi.org/10.1021/acs.molpharmaceut.4c00166
Mol. Pharmaceutics 2024, 21, 2590−2605

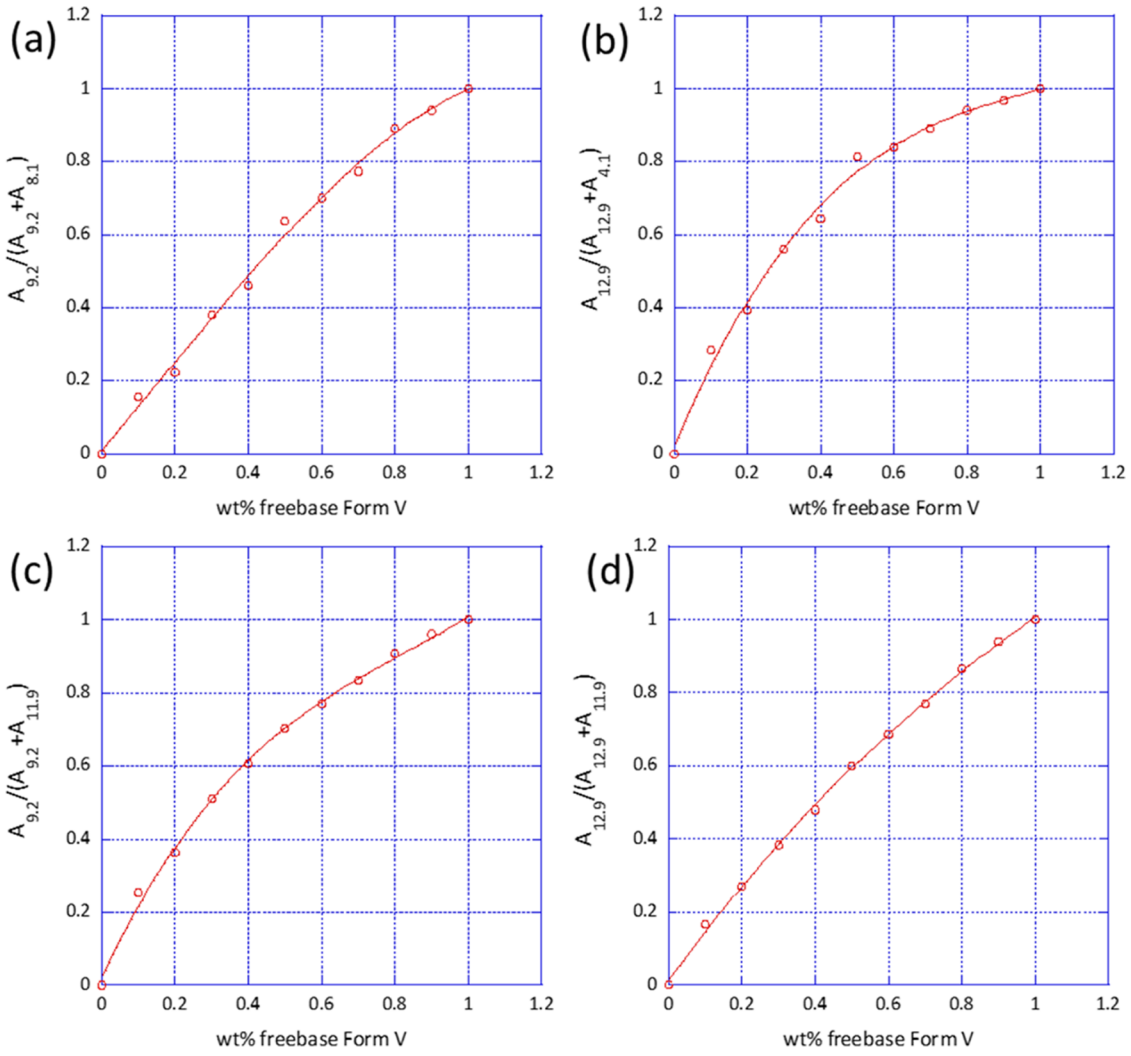

Figure 3. X-ray calibrations of maleate and freebase Form V binary mixtures. A_q represents the integrated area of the specified 2q peak position (e.g., 8.1, 9.2, 11.9°): (a) $y = 0.007914 + 1.202x + 0.1308x^2 - 0.3419x^3$, (b) $y = 0.01983 + 2.372x - 2.080x^2 + 0.6864x^3$, (c) $y = 0.01950 + 2.144x - 1.946x^2 + 0.7925x^3$, (d) $y = 0.01309 + 1.377x - 0.4748x^2 + 0.09195x^3$.

performance liquid chromatography−ultraviolet (UPLC-UV). Intrinsic dissolution results are reported as average IDR (±SD) over three experiments (n = 3). A graph of the accumulated amount of dissolved API (mg/cm^2) vs time (min) is constructed, and a linear regression of the curves to obtain the slope is reported as the calculated IDR.

2.3.5. Kinetic Solubility Measurement. The kinetic solubility of HCl salt, maleate, and freebase Form V was determined at room temperature in simulated intestinal fluid (SIF) prepared at pH 5.0. SIF at pH 5.0 is commonly evaluated by the authors to determine if any differences in a compound's FaSSIF vs FeSSIF solubility are driven by the presence of bile salts or simply lower pH. Approximately 50 mg freebase equivalent of the API was added to 50 mL of SIF pH 5.0 and stirred at low speed using a magnetic stir bar. Samples were drawn at specific time points and filtered through a syringe-driven filter. The filtrate samples were analyzed by UPLC-UV using an internal API assay method. The residual solid isolated from the filtration process was analyzed by X-ray diffraction for form composition determination.

3. RESULTS AND DISCUSSION

3.1. Crystal Structure of Various Solid Forms. While amorphous or disordered solids were obtained as mesylate, tosylate, sulfate, and oxalate, only three salt/cocrystal forms (HCl, maleate, and fumarate) were crystalline and deemed suitable for evaluation after extensive screening. Each material was grown to an appropriate size to afford single-crystal analysis. The crystal structure of the maleate had been previously reported.[51] Here, we present the local structures of maleate, HCl, and fumarate, specifically near the region of API/acid interaction (Figure 4). Several implications were noted from the structural elucidation:

- The FDA guidance[8] offers the opinion that if the API and its coformer have a $\Delta pK_a > 1$ with substantial proton transfer, the ionization will lead to the formation of a salt instead of a cocrystal. This criterion qualifies maleate and HCl as salts, as the tertiary amine of the molecule has a measured pK_a of ∼3.7. On the contrary, the triazole moiety of the API with pK_a of ∼1.2 makes fumarate a cocrystal through hydrogen bonding.

https://doi.org/10.1021/acs.molpharmaceut.4c00166
Mol. Pharmaceutics 2024, 21, 2590−2605

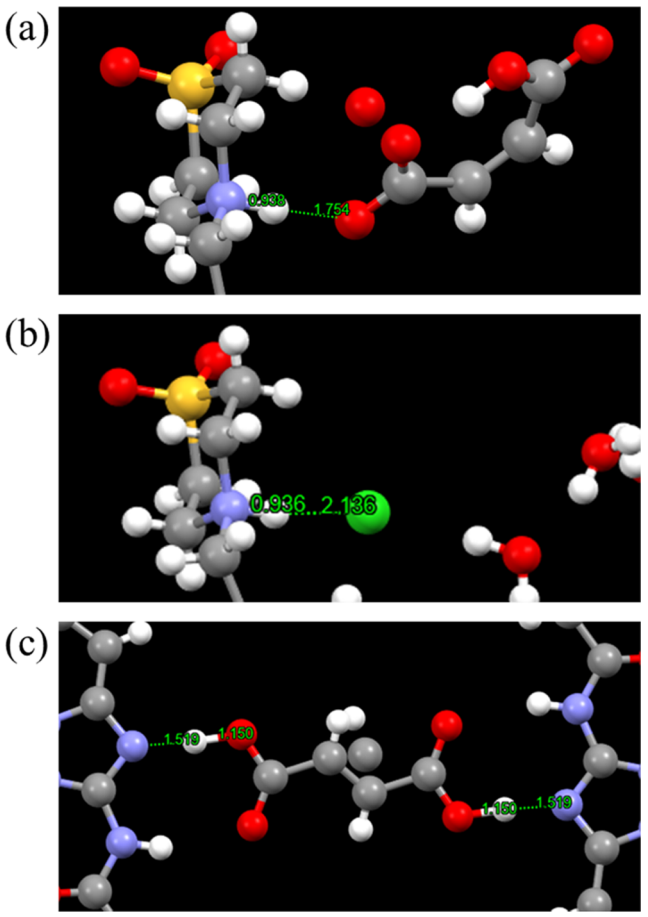

Figure 4. Partial atomic displacement ellipsoid drawing with molecular interaction between Compound X freebase and (a) maleic acid, (b) HCl, and (c) fumaric acid.

- The electron density distribution and the bond length estimated from the Crystallographic Information File (.cif) suggest complete proton transfer in maleate and HCl salt. However, the fumaric acid still retains the proton (O4···H4 = 1.150 Å vs H4···N2 = 1.519 Å), agreeing with the anticipation based on pK_a difference.
- The crystal structure of the fumarate contains two molecules of API with one molecule of fumaric acid (pK_a = 3.0). Figure 4(c) shows both ends of the fumaric acid are engaged in hydrogen bonding, making it a hemifumarate cocrystal.
- Additional screening with a range of stoichiometric ratios (from 0.5 to 2.5 acid/API molar equivalence) did not lead to the formation of other salts/cocrystals (e.g., di-HCl salt, hemimaleate, monofumarate, or conjugate acid−base cocrystal).

Direct comparison of salt and cocrystal properties is impractical due to different chemical compositions and the natural distinction in strength between ionic and hydrogen bonds. However, the molecular conformations suggest that hemifumarate has the most robust packing among the three. The HCl salt has the lowest calculated density of 1.351 g/cm^3 (derived from the content (mass) per unit cell volume). The maleate and hemifumarate have higher and comparable densities of 1.445 and 1.424 g/cm^3, respectively. The hemifumarate is particularly unique as all possible (4) hydrogen bonds to and from the fumaric acid are being formed, making it a relatively stable structure. In the case of the maleate, the acid has only one hydrogen bond to the API, and the other end of the maleic acid does not join the API or hydrogen bond to anything other than itself. Despite the marginally higher density, the maleic acid is not actively involved in the structural network. Therefore, it is expected to be less robust in crystallography terms. These qualitative rationales for the three solid forms will be verified by physical property assessments, as shown in the subsequent sections.

3.2. Solid Form Options for Development. Salts are viable options to counter the solubility challenges with the BCS Class II classification of Compound X. HCl salt, in particular, holds an advantage due to its GRAS status and its common use in marketed products. Many maleate salts have also been approved for oral administration, with a maximum daily intake as high as 250 mg in acetophenazine hydrogen maleate.[13] However, kidney damage has been reported as a systemic toxic action in rats and dogs with low adverse effect level (LOAEL) at 100 mg/kg. For Compound X, both HCl and maleate are feasible for pharmaceutical development.

Figure 5 shows the intrinsic dissolution rate (IDR) of the relevant forms. Freebase Form V has the lowest IDR with 12.7 μg/min/cm^2 in 0.01 N HCl (pH 2) and 0.76 μg/min/cm^2 in 20 mM phosphate buffer (pH 6.8). HCl salt has the highest

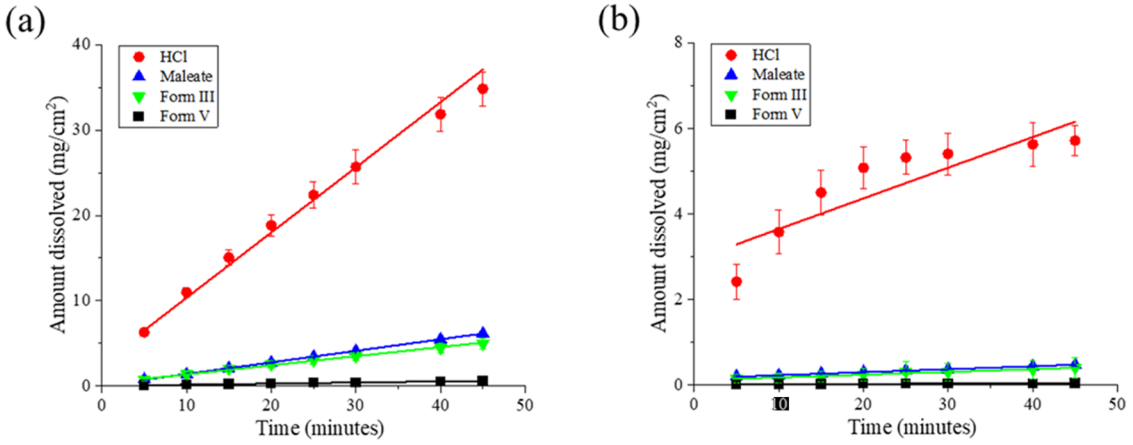

Figure 5. Dissolution of various forms at 37 °C in (a) 0.01 N HCl (pH 2) and (b) 20 mM phosphate buffer (pH 6.8). The slopes of the curves are the IDR in mg/min/cm^2.

https://doi.org/10.1021/acs.molpharmaceut.4c00166
Mol. Pharmaceutics 2024, 21, 2590−2605

Table 1. Pharmacokinetic Profiles of Compound X and Its Metabolite (X′) in Plasma of Beagle Dogs Following an Oral Dose of 100 mg Fixed Tablet (Mean ± Standard Deviation, n = 6)

famotidine-pretreated dog	HCl		maleate	
dose (mg)	100 freebase equivalent		100 freebase equivalent	
analyte	X	X′	X	X′
$T_{1/2}$ (h)	12.6 ± 12.0	>24	13.4 ± 10.4	>24
T_{max} (h)	0.63 ± 0.31	12.3 ± 9.07	1.13 ± 0.74	15.3 ± 9.52
C_{max} (μM)	4.97 ± 2.21	0.75 ± 0.27	5.28 ± 2.57	0.99 ± 0.43
AUC_{last} (μM·h)	34.7 ± 11.8	12.7 ± 6.08	35.1 ± 14.5	16.4 ± 6.92

IDR with 764 μg/min/cm^2 and 71.7 μg/min/cm^2 in pH 2 and 6.8 dissolution media, respectively. The IDRs are comparable for the maleate and freebase Form III, a metastable and transient form. At pH 2, the IDR is 135.4 and 107.0 μg/min/cm^2 for the maleate and Form III, respectively. At pH 6.8, the IDR is 7.0 and 6.4 μg/min/cm^2, respectively. The IDR results suggest that the HCl salt is the most attractive candidate, with maleate as a potential alternative. Freebase Form III has a solubility similar to the maleate's; however, its metastable nature precludes it from being considered as a practical option.

The HCl salt and maleate were further compared in a preclinical study where their pharmacokinetic performance was evaluated using identical tablet formulations and dosed in fasted, famotidine-pretreated dogs (n = 6) at 100 mg freebase equivalent. Both salts exhibited similar exposure of Compound X and Compound X', the active metabolite, with respect to AUC, C_{max}, and T_{max} (Table 1). The pharmacokinetics demonstrated by the two salts did not provide meaningful differentiation in performance. However, the physical stability of the HCl salt, specifically the trihydrate structure and dehydration risks under low relative humidity conditions, causes concern about its suitability for commercial use. In subsequent sections, the two salts will be appraised from the perspective of disproportionation liability, which may compromise the performance of the drug.

3.3. Disproportionation of Salts in Aqueous Conditions. *3.3.1. Disproportionation Mechanism.* The kinetics of the forward reaction (salt formation) of Compound X had been previously reported.[51] The reverse process (disproportionation) is graphically represented in Figure 6. The polymorph landscape has made the investigation challenging due to the presence of multiple freebase forms. There were observations on relative stability from various experiments, as indicated by the arrows in Figure 6, but the dynamics and transient nature of Forms I, II, and III suggest these transformations do not always follow the Ostwald rule of stages.[52] Freebase Form V is the most thermodynamically stable among the group, with all other forms eventually converging to Form V.

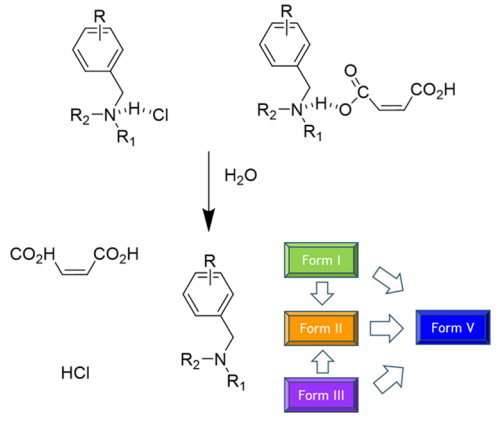

Figure 6. Disproportionation process for the HCl salt and maleate. The arrows indicate transformation paths that have been observed.

3.3.2. Disproportionation Kinetics of the Maleate and HCl Salts. HCl salt at a 25 mg/mL concentration will be used as an example for demonstration purposes. The sampling cadence varies but typically starts from 5 min and then decreases over time. Most of the transformations took place within the first 2 h. Table 2 shows the quantitation of the process, with disproportionation commencing at time zero (pure salt in water). Slurry samples were isolated and analyzed by X-ray, and the relative composition of binary pairs (e.g., HCl salt vs Form II, Form II vs Form V) was determined. The ratios were then combined and normalized following eq 5, where 0 denotes the input (salt) and 1/2/3/4 indicates freebase Forms I/II/III/V, respectively.

Table 2. Quantitation of Solid Forms in the Disproportionation Process of HCl Salt at 25 mg/mL

sample	time (min)	salt X_0	FB form I X_1	FB form II X_2	FB form III X_3	FB form V X_4
1	0	1	0	0	0	0
2	5	0.32	0.23	0.46	0	0
3	10	0.19	0.22	0.59	0	0
4	20	0.10	0.18	0.43	0	0.29
5	35	0.06	0.02	0.57	0	0.34
6	50	0	0	0.50	0	0.50
7	82	0	0	0.40	0	0.60
8	112	0	0	0.34	0	0.67
9	173	0	0	0.13	0	0.87
10	234	0	0	0	0	1
11	351	0	0	0	0	1
12	416	0	0	0	0	1

$$X_0 + \sum_{i=1}^{4} X_i = 1 \tag{5}$$

It should be noted that for any binary pairs, different calibration curves in Figure 3 lead to slightly different results, but the variability is insignificant (≤2−3%).

Figure 7 is a bar chart showing the disproportionation kinetics of HCl salt at 40 (mL/g) volume/weight ratio (25 mg/mL). While freebase Form III was occasionally observed in solubility studies, it is absent from all disproportionation experiments, conceivably attributed to its transient and metastable nature. Both Form I and Form II were observed in the initial stage of this experiment. The amount of Form I decreased as time progressed, suggesting Form I either converted to Form II, then to Form V, or it converted directly to Form V, which started to emerge at about the 20 min mark.

https://doi.org/10.1021/acs.molpharmaceut.4c00166
Mol. Pharmaceutics 2024, 21, 2590−2605

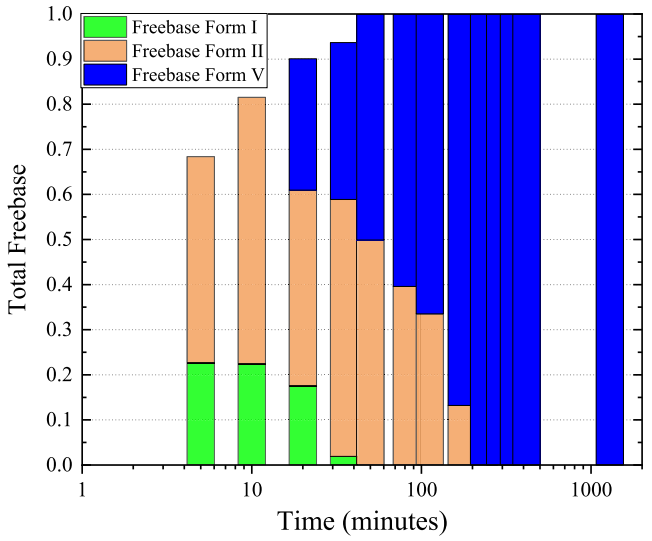

Figure 7. Disproportionation kinetics of HCl salt in pure water at 25 mg/mL. The *X*-axis was changed to a logarithmic scale for better visualization.

Form II increased in the first 10 min. Its growth was suppressed upon the emergence of Form V and eventually faded with continuous conversion to Form V, the most stable polymorph.

It is worth noting that X-ray quantitation is operationally straightforward yet labor-intensive. Integrating featured X-ray peaks, calculating the composition of binary mixtures via calibration curves, and normalizing the results through eq 5 all contribute to a manually demanding task. We turned to PAT Raman to collect the kinetic data in a continuous manner. As previously reported,[51] the salt formation can be effectively tracked by Raman spectroscopy as only two forms (freebase Form V and salt) are involved, and first-principles analysis by peak integration is adequate to extract the kinetic details. For the disproportionation process, the salt and freebase forms lead to highly convoluted spectra; thus, direct quantitation by peak integration is no longer practical. Figure 8 is an example of the time evolution of Raman spectra as disproportionation progresses. The transformations could be visualized qualitatively; however, a direct kinetic analysis was not possible. There is no region in the spectra where distinct peaks from individual forms do not overlap with one or more of the other forms. Therefore, detailed quantification of the kinetics requires a significantly more sophisticated methodology.

Form quantitation by Raman spectroscopy requires chemometric methods to address overlapping peaks. Specifically, partial least-squares (PLS) modeling was used in which the unique covariance structures associated with each form were extracted from the entire spectra. We used offline X-ray measurements as a reference during model development. The concept of using a single disproportionation run to generate quantitative Raman models has been reported previously.[48] We used this approach to characterize the disproportionation kinetics for the HCl salt and maleate to verify X-ray diffraction measurements further and to enhance our mechanistic understanding of salt behaviors.

The model performance and metrics are captured in Figures 9−10 and Table 3. Figure 9 shows the Raman polymorph predictions overlaid with the X-ray measurement values across each concentration for the HCl salt. The quality of the match (Raman vs X-ray) can be assessed by the R^2 values in Table 3, which were greater than or equal to 0.95. In addition to the model fit, the errors of the Raman models were evaluated using RMSEC and RMSECV. The RMSEC shown in Table 3 ranged from 0.006 to 0.062 weight fractions across the models generated for the HCl salt at different concentrations. The highest error was associated with the Form V model at 50 mg/mL concentration. This result was also supported by cross-validation metrics. The RMSECV for HCl salt disproportionation ranged from 0.011 to 0.122 weight fractions, where the highest RMSECV of 0.122 weight fraction was also associated with the Form V model at 50 mg/mL concentration. This relatively higher error can be attributed to the narrower weight fraction range of Form V used in model development from a partial disproportionation run. A more comprehensive assessment of concentration and solid form effects on quantitative Raman model development for this system is highlighted in our previous work.[48]

Similar to the HCl salt disproportionation, the Raman models generated on maleate disproportionation had high correlation coefficients and low errors. The R^2 values were again 0.95 or greater, showing a good fit with Raman predictions and X-ray quantitation values. The RMSEC and RMSECV ranged from 0.002 to 0.021 and 0.003 to 0.030 weight fractions, respectively. These models were more accurate than the ones developed for HCl salt disproportionation due to a more straightforward polymorph system with

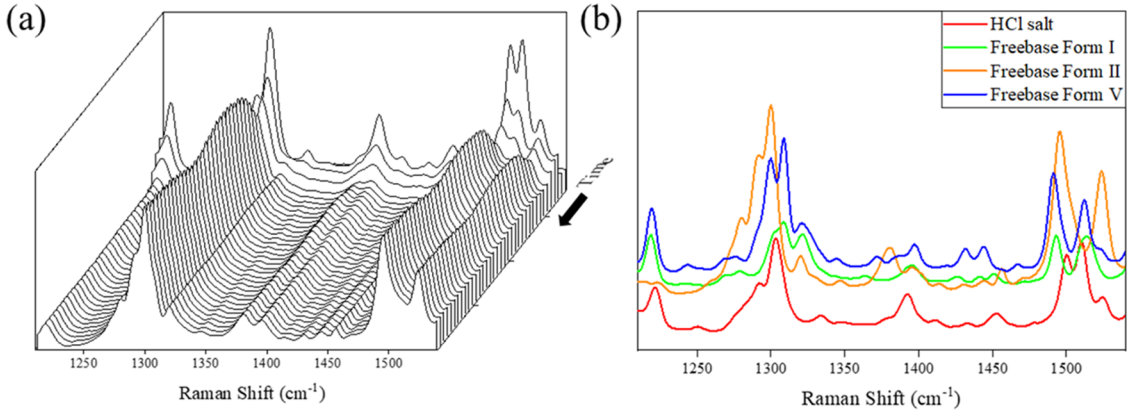

Figure 8. (a) Time evolution Raman profile for a typical HCl salt disproportionation. (b) Reference spectra of pure forms related to the process.

https://doi.org/10.1021/acs.molpharmaceut.4c00166
Mol. Pharmaceutics 2024, 21, 2590−2605

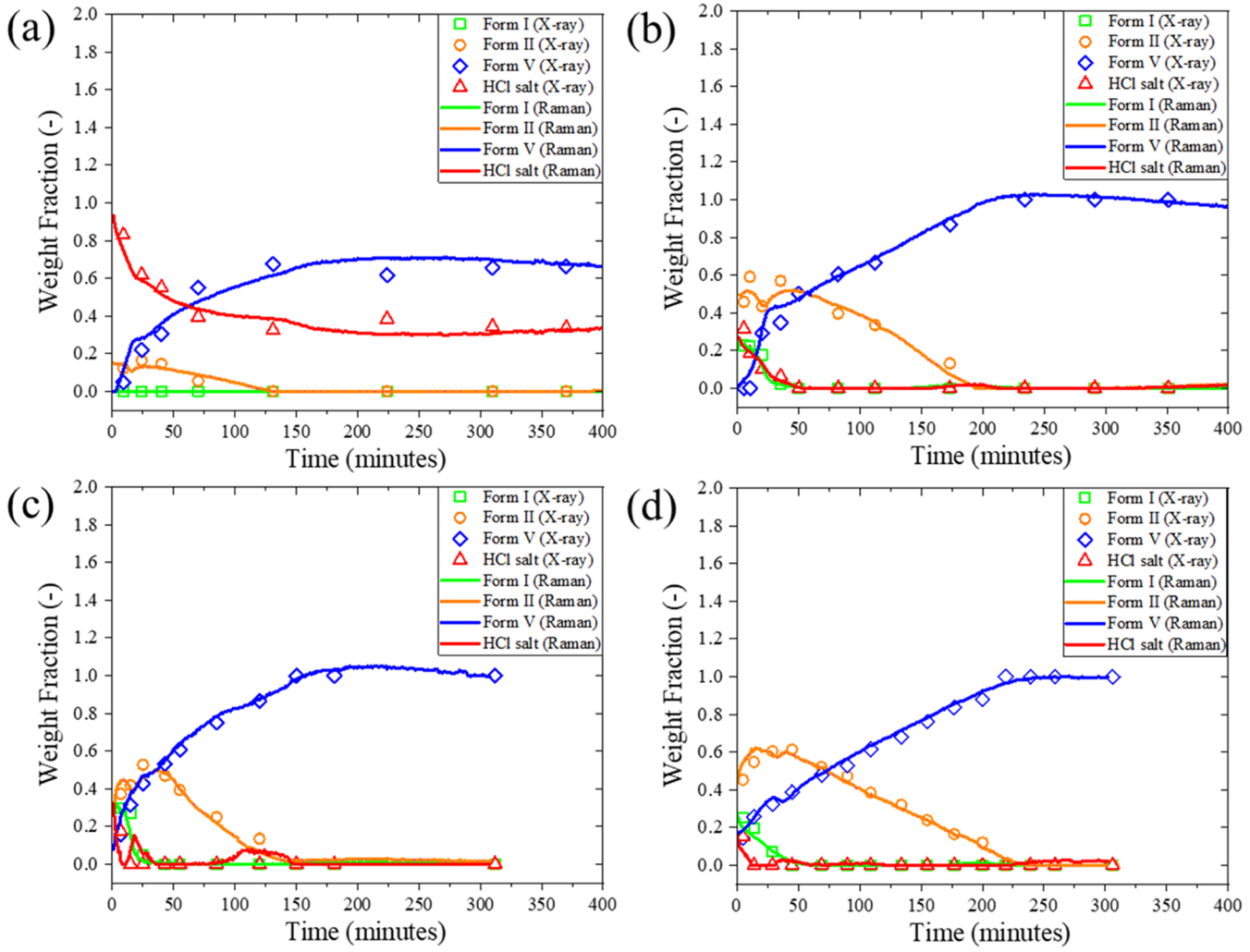

Figure 9. Disproportionation kinetics at various concentrations for HCl salt: (a) 50 mg/mL, (b) 25 mg/mL, (c) 16.7 mg/mL, and (d) 12.5 mg/mL. Complete disproportionation was observed in all cases except for the 50 mg/mL concentration.

only two forms (Form II and Form V) as opposed to three forms (Form I, Form II, and Form V) in the HCl salt system. The high accuracy of the Raman models for both HCl salt and maleate disproportionation suggested that the appearance and disappearance rates of various polymorphs can be reliably evaluated to extract kinetic rate constants.

The kinetic rates of the more dominant Form II and Form V were assessed for each disproportionation run. First-order kinetics were assumed at the time range of approximately 50 to 150 min. The linear rates at this range for both the HCl salt and maleate disproportionation runs are summarized in Table 4. For HCl salt disproportionation, the first-order assumption was applicable based on the high linear fit ($R^2 > 0.95$). The Form V growth rate increased from 0.0026 to 0.0037 weight fractions per minute as the solid concentration decreased from 50 to 16.7 mg/mL. The conversion rate seemed to plateau at lower solid concentrations. This was complemented by a decreasing rate of Form II formation from −0.0014 to −0.0053 weight fractions per minute. At the end of HCl disproportionation, most runs reached near-complete disproportionation, except for runs with a 50 mg/mL concentration. At the end of the 50 mg/mL run, approximately 0.64 weight fractions of Form V were present, with about 0.01 Form II and 0.35 HCl weight fractions remaining in the system.

The kinetic rates for maleate disproportionation were 1 order of magnitude lower than that of the HCl salt. These rates were calculated based on the assumption of first-order kinetics. However, the R^2 of the linear fit was relatively low (0.60−0.99) in most cases. The deviation from first-order kinetics could be due to the insignificant growth or disappearance rates of the polymorphs. The slow linear rates are shown in Table 4 for Form V and Form II and ranged from −0.00006 to 0.00030 weight fractions per minute. None of the maleate runs reached complete disproportionation, with the highest level of Form V being only 0.15 at the end of the 16.7 mg/mL run. These results clearly showed that maleate was more stable than the HCl salt.

The Raman models gave us continuous kinetic profiles of the process and an opportunity to cross-examine the accuracy of form quantitation by X-ray. For better visualization and ease of comparison through trending lines, we will only graph discrete X-ray data points in the discussions below.

3.3.3. Implications of the HCl and Maleate Salt Disproportionation. Significant differences were observed in the magnitude of disproportionation between the HCl salt and the maleate. Figure 11 shows the kinetic profiles of the two salts at four concentrations. These stress experiments were performed in a closed aqueous system with no additives. The

https://doi.org/10.1021/acs.molpharmaceut.4c00166
Mol. Pharmaceutics 2024, 21, 2590−2605

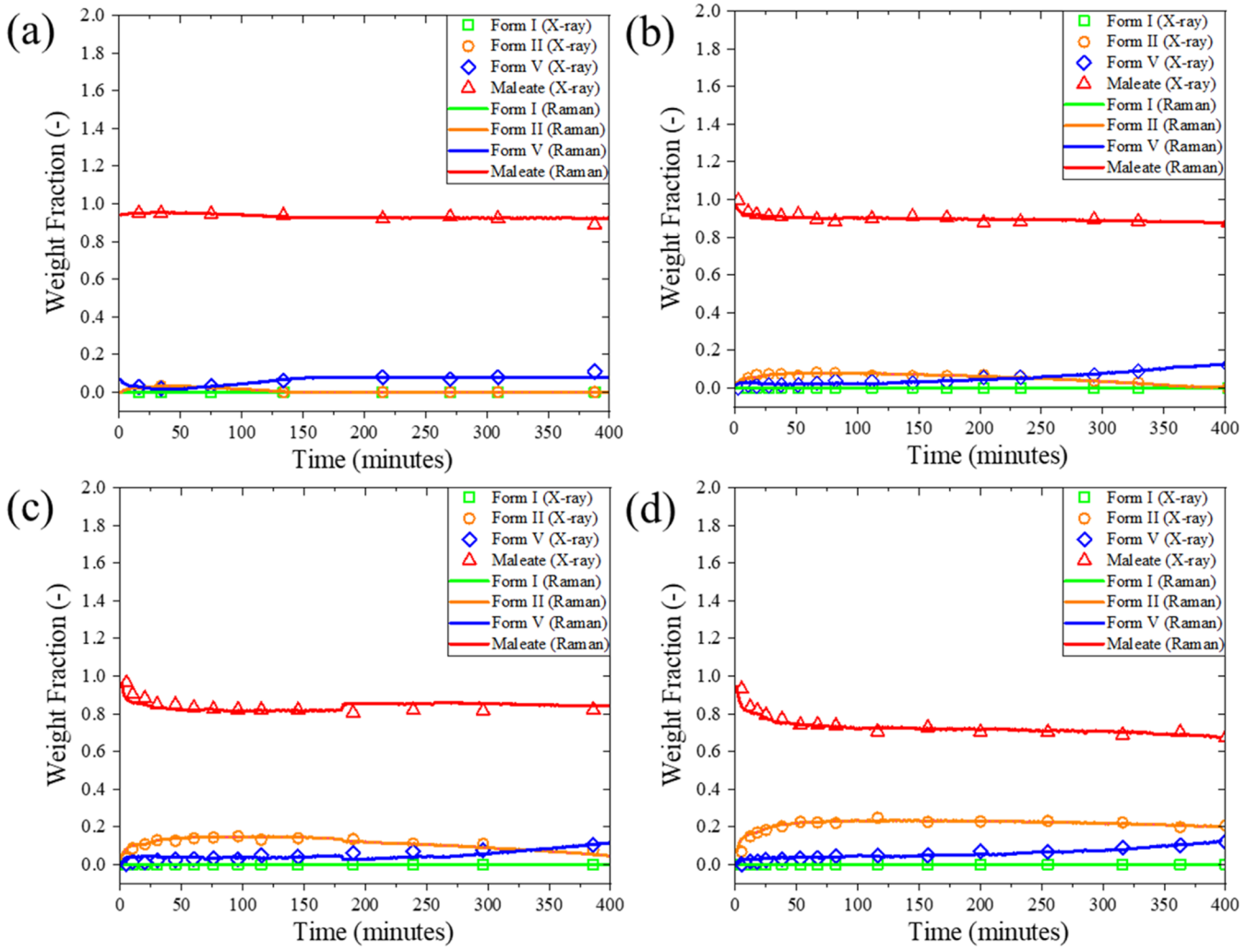

Figure 10. Disproportionation kinetics at various concentrations for maleate: (a) 50 mg/mL, (b) 25 mg/mL, (c) 16.7 mg/mL, and (d) 12.5 mg/mL. Note that freebase Form I was not observed in any cases.

Table 3. Model Metrics (RMSEC, RMSECV, and R^2) for the Raman Models for the HCl Salt and the Maleate

		HCl			maleate		
		RMSEC	RMSECV	R^2	RMSEC	RMSECV	R^2
50 mg/mL	form I	n/a	n/a	n/a	n/a	n/a	n/a
	form II	0.022	0.068	0.95	0.002	0.003	0.96
	form V	0.062	0.122	0.95	0.014	0.027	0.98
25 mg/mL	form I	0.006	0.011	0.99	n/a	n/a	n/a
	form II	0.043	0.059	0.97	0.007	0.014	0.97
	form V	0.046	0.076	0.98	0.008	0.017	0.97
16.7 mg/mL	form I	0.006	0.061	0.99	n/a	n/a	n/a
	form II	0.041	0.052	0.98	0.011	0.016	0.98
	form V	0.014	0.024	0.98	0.021	0.030	0.99
12.5 mg/mL	form I	0.013	0.029	0.99	n/a	n/a	n/a
	form II	0.020	0.031	0.97	0.007	0.010	0.98
	form V	0.023	0.051	0.98	0.008	0.013	0.98

HCl salt breaks down completely (except at 50 mg/mL) within 20 min. The maleate, however, retains most of the input under all conditions evaluated. The difference is consistent with our anticipation. An estimate of pH_{max} based on eqs 1 and 2 indicated pH_{maxHCl} is ca. 0.3, while $pH_{maxmaleate}$ is ca. 1.1. The lower pH_{max} of the HCl salt translates to a much narrower biorelevant pH range under which the ionized species is thermodynamically stable.

The disparity between the two salts has implications for the liability of the HCl salt. Despite satisfactory dog PK (Table 1) and superior intrinsic dissolution (Figure 5), the propensity of the HCl salt to disproportionate is an inherent risk that

https://doi.org/10.1021/acs.molpharmaceut.4c00166
Mol. Pharmaceutics 2024, 21, 2590−2605

Table 4. Linear Rates for Form V and Form II from the Raman Models

linear rates		HCl			maleate		
		rate (wt fraction/min)	R^2	end wt fraction	rate (wt fraction/min)	R^2	end wt fraction
form V	50 mg/mL	0.0026	0.97	0.64	0.00010	0.60	0.07
	25 mg/mL	0.0033	0.99	0.95	0.00030	0.92	0.13
	16.7 mg/mL	0.0037	0.97	0.99	0.00020	0.74	0.15
	12.5 mg/mL	0.0037	0.99	0.99	0.00020	0.90	0.12
form II	50 mg/mL	−0.0014	0.99	0.01	−0.00030	0.99	0.0005
	25 mg/mL	−0.0028	0.99	0.03	−0.00006	0.66	0.0012
	16.7 mg/mL	−0.0053	0.99	0.01	0.00008	0.66	0.0195
	12.5 mg/mL	−0.0034	0.99	0.00	0.00010	0.72	0.2012

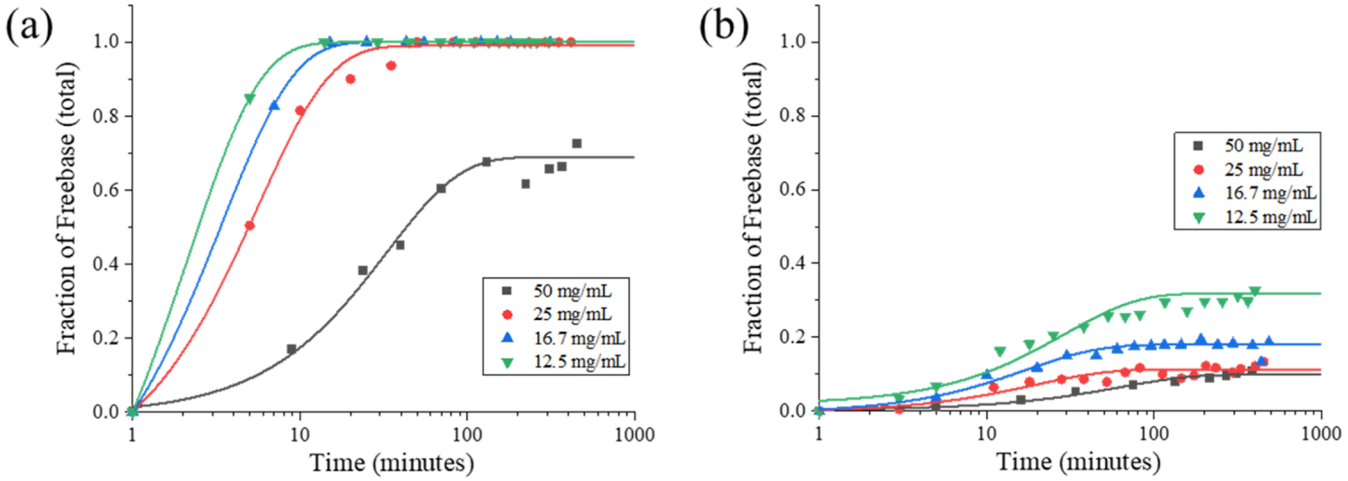

Figure 11. Disproportionation kinetics at various concentrations for (a) HCl salt and (b) maleate. The *y*-axis represents the total amount of freebase (Forms I, II, and V combined).

undermines its suitability for product use (e.g., stability during storage).

Kinetic solubility measurements revealed additional details of the HCl salt's solubility behavior (Figure 12). While the HCl salt was fully comparable to the maleate initially, disproportionation started to occur at ca. 40 min, causing a sudden drop of solubility to the freebase level, a highly undesirable "spring-free-fall" scenario. Solid recovered at the end was consistent with pure freebase (complete disproportionation). By comparison, the maleate continued to maintain a high solubility throughout the measurement. Also included in Figure 12 is the kinetic solubility profile of the hemifumarate, which generated a lower supersaturation (~5-fold) than the HCl or maleate, but remained disproportionation-free in the same time frame.

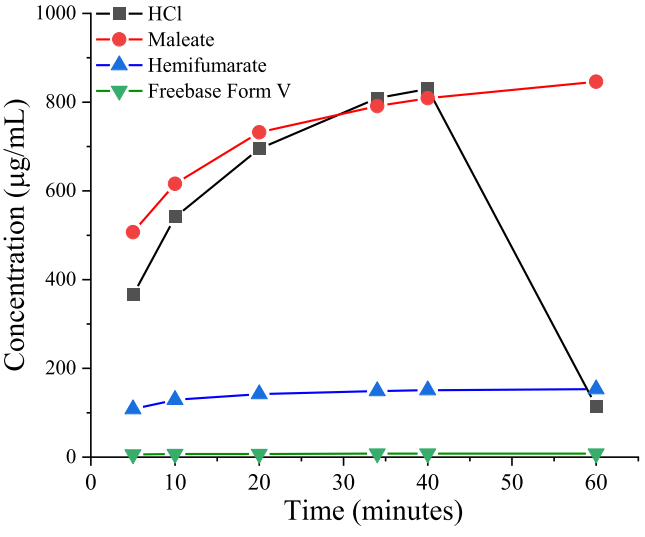

Figure 12. Kinetic solubility of the HCl salt, maleate, hemifumerate, and freebase in SIF (pH = 5.0) at 20 °C.

Under separate settings (pure water vs SIF) and concentrations, HCl salt consistently leads to an earlier onset of disproportionation, suggesting a higher risk of freebase precipitation that would limit drug absorption in the gastrointestinal tract. Maleate, on the other hand, shows robustness and maintains the higher concentration needed to ensure drug product performance.

3.3.4. Assessment of the Hemifumarate. We had projected hemifumarate to be a stable structure due to its heavily engaged hydrogen bonding. In addition to higher crystal density, the superior stability of the hemifumarate is also reflected by its better resistance to disproportionation during kinetic solubility measurement (Figure 12). Additionally, thermal properties, as characterized by differential scanning calorimetry (DSC), show HCl salt's loss of crystallinity upon dehydration at a relatively low temperature (ca. 50−125 °C), while the hemifumarate remains intact up to ca. 250 °C where it melts and decomposes simultaneously. From the perspective of the onset temperature to activate a melting event or the energy required to break the structure (heat of fusion), the thermal data imply that hemifumarate is uniquely sturdy among the group (Figure 13).

https://doi.org/10.1021/acs.molpharmaceut.4c00166
Mol. Pharmaceutics 2024, 21, 2590−2605

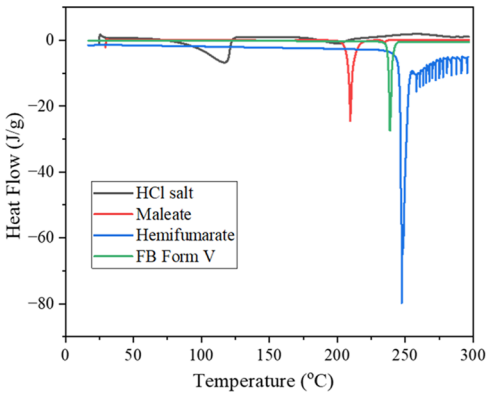

Figure 13. Differential scanning calorimetry (DSC) profiles of various forms. HCl salt has an early dehydration event. TG-MS data (not shown) confirms loss of water from approximately 25 to 100 °C and the loss of HCl from approximately 100 °C onward. The sharp endotherms of the maleate (onset 208.3 °C, peak 209.6 °C) and hemifumarate (onset 246.0 °C, peak 247.4 °C) are accompanied by major weight loss (>20%,) due to decomposition. Freebase Form V is also included for reference.

There has been an extensive survey of salt and cocrystal solubility, and the popular notion that salt is typically more soluble.[53] We recognized that the comparison could be situational and governed by factors such as pH_{max}, supersaturation index, and K_{sp}/K_a.[53] Mathematical models have been derived to predict the solubility/supersaturation dependence and thermodynamic stability as a function of solution pH. Within the scope of this investigation, it is prudent to assume that hemifumarate has the lowest solubility both kinetically and thermodynamically among the three salts/cocrystals investigated.

Hemifumarate's superior stability is best demonstrated by the disproportionation profiles of Figure 14, where all three salts/cocrystals at 12.5 mg/mL concentration were subject to the stress condition of 50 °C in pure water. Hemifumarate

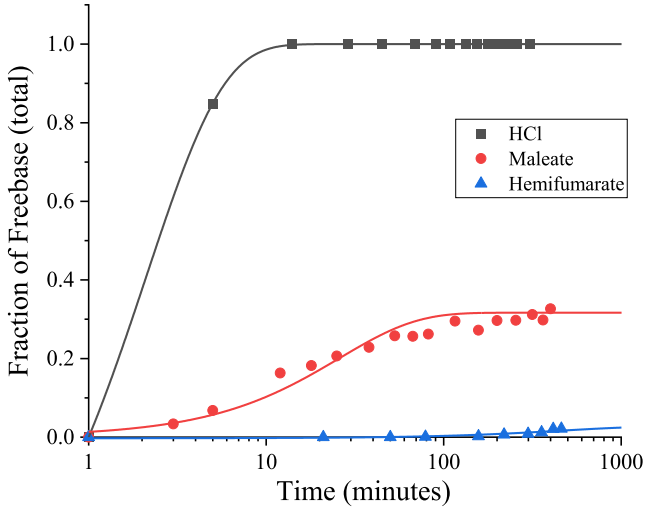

Figure 14. Disproportionation kinetics of HCl salt, maleate, and hemifumarate at 12.5 mg/mL concentration and 50 °C. The *y*-axis represents the total amount of freebase. At the end of the experiment, disproportionation is at ca. 100, 30, and 3% for HCl salt, maleate, and hemifumarate, respectively.

distinguished itself with a significantly lower level (<5%) of disproportionation after 24 h.

3.4. Solid Form Selection for Pharmaceutical Development. The physical property and disproportionation behavior in previous sections were evaluated to determine the appropriate form for further development. The HCl salt was disfavored due to the labile trihydrate structure (dehydrates at RH < 20%) that would require active control of temperature and humidity during manufacturing and storage, which is logistically possible but undesirable. More critically, the propensity of the HCl salt to disproportionate was deemed too high of a risk, as it would likely introduce significant variability in performance and stability.

The lower solubility of the hemifumarate and its kinetic solubility profile suggested that hemifumarate was not an ideal form for development, despite its notable physical stability and resistance to disproportionation.

Among the three salt/cocrystal options, the maleate had the most balanced characteristics: dissolution nearly equivalent to the HCl salt and physical stability comparable to hemifumarate. Extensive polymorph screening of the maleate has confirmed a single polymorph—a stable hemihydrate that remains structurally intact even in the absence of water. The stability and manufacturing flexibility make it an attractive candidate to be used as the API. Based on the above consideration and the favorable preclinical pharmacokinetics profile observed in famotidine-treated dogs (Table 1), a tablet formulation of the maleate was selected for further clinical development. Research focus was shifted to the optimization of the formulation to address and minimize the potential impact of salt disproportionation on drug products.

3.5. Formulation Optimization. *3.5.1. Microenvironmental pH Modulation.* Microenvironmental pH modulation using a pH modifier proves to be the most effective method to suppress disproportionation and achieve pH-independent solubility. The approach aims to extend the supersaturation locally to prevent the precipitation of the neutral form. For weak base drugs, frequently used acid modifiers include (in descending pK_a) sorbic acid (4.8), succinic acid (4.2), ascorbic acid (4.2), malic acid (3.4), citric acid (3.1), fumaric acid (3.0), and tartaric acid (3.0).[34,38] The selection of a pH modifier is typically not straightforward, because of the interplay of multiple factors involved in the mechanism. It is generally hypothesized that the pH modifier dissolves in the moisture layer surrounding the particles and creates a solution that favors supersaturation of the drug. Thus, the pH in the solid phase (and consequently the diffusion layer) is dependent on the pK_a of the modifier. The rationale also implies that bringing the pK_a of the modifier close to the pH_{max} of the API would be favorable. However, this is not always feasible given the relatively narrow pK_a range (ca. 2.9−4.8). Lastly, the aqueous solubility and concentration of the modifier, its dissolution rate, and how it is integrated into the formulation will all influence the success of microenvironmental pH control. Numerous studies have compared the effectiveness of acid modifiers.[31,32,34,38] Still, the most optimal choice often hinges on several factors mentioned above to suit the unique physiochemical properties of the drug molecule.

3.5.2. Synergistic Benefit of Fumaric Acid as the Modifier. To minimize maleate disproportionation and ensure sufficient solubilization throughout the delivery and absorption cycle, we resorted to pH modulation to generate favorable micro-

https://doi.org/10.1021/acs.molpharmaceut.4c00166
Mol. Pharmaceutics 2024, 21, 2590−2605

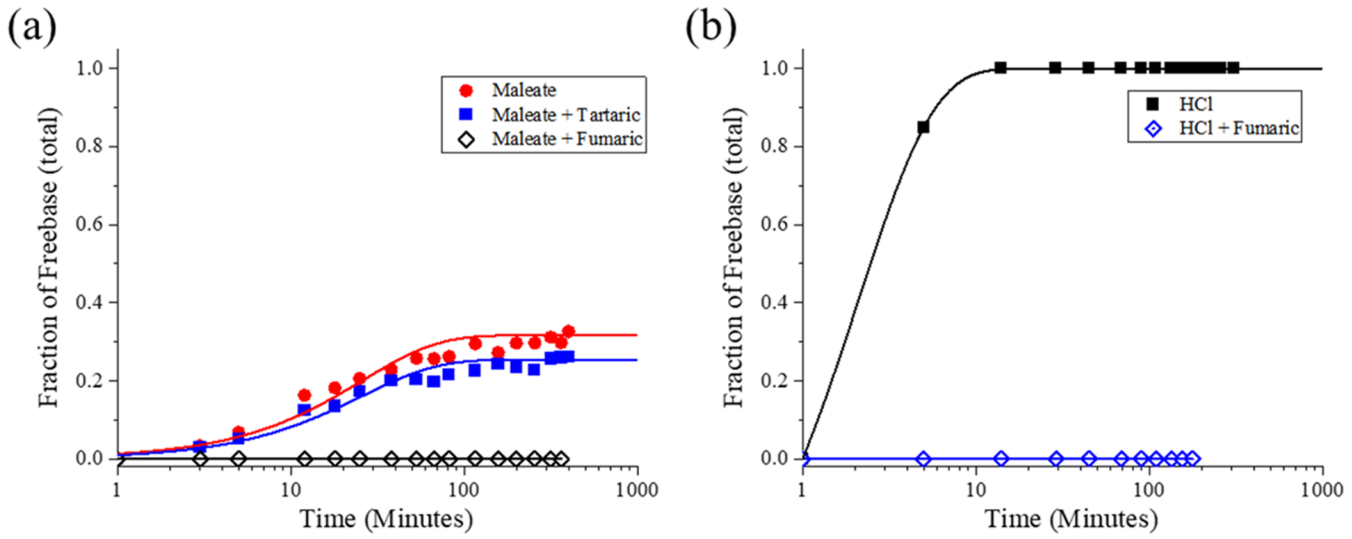

Figure 15. Effect of fumaric acid or tartaric acid on the disproportionation kinetics: (a) maleate with tartaric and fumaric acids and (b) HCl salt with fumaric acid. No freebase was observed in both cases when fumaric acid was added to the aqueous slurry of salts.

environmental pH. In designing the formulation composition, fumaric acid was selected among the group of acid modifiers. Its moderate aqueous solubility is advantageous in matching the pace of the drug release, thus providing continuous availability to regulate pH_M for a longer duration.[37,54] We also intended to leverage the cocrystal-forming capability of fumaric acid. Its presence provides a secondary opportunity to create a high solubility species when freebase is generated from the breakdown of the salt. To the best of our knowledge, there have not been precedents of using a pH modifier for dual purposes—to modulate pH_M, and to scavenge and bind the loose freebase to keep solubility at a high level.

A study to explore the effectiveness of fumaric acid as a pH modulator was undertaken. A disproportionation stress test at 12.5 mg/mL was performed using maleate, maleate with fumaric acid, and a control using maleate with tartaric acid (Figure 15). Fumaric acid was set at 5% of the tablet weight, a typical proportion in published formulation compositions where an acid modifier is utilized. The disproportionation profile was dramatically changed, with no freebase observed throughout the experiment. Figure 15 shows a head-to-head comparison with and without fumaric acid. The difference aligns with our design strategy—to eliminate disproportionation completely.

The critical role of fumaric acid is further demonstrated by the control experiment, where tartaric acid was used in place of fumaric acid. Tartaric acid has a pK_a identical to that of fumaric acid (3.0). The acidity of an aqueous solution at 25 °C is essentially the same—fumaric (pH = 2.15) vs tartaric (pH = 2.2),[55] offering the closest match among all acid modifiers. Figure 15 shows that the addition of tartaric acid reduces the level of disproportionation; however, the reduction was marginal. Tartaric acid does not have the same synergistic benefit offered by fumaric acid to minimize disproportionation due to the lack of a corresponding crystalline tartrate salt. Mechanistically, including fumaric acid in the formulation is designed to modulate microenvironmental pH. Once the fumaric acid is released, it functions as a freebase scavenger by combining with the freebase and forming the hemifumarate. This keeps the solubility of the system no lower than the hemifumarate solubility. Hypothetically, the free maleic acid can continue to serve the role of acid modifier and create a favorable pH for the formulation. This mechanism does not exist in the case of tartaric acid, which merely alters (minimally) the pH of the bulk solution but is not actively engaged in the prevention of freebase precipitation. It is worth noting that at the end of the stress experiment in Figure 15, the pH values of the aqueous slurry are 1.8 (maleate), 1.7 (maleate + fumaric acid), and 1.7 (maleate + tartaric acid), respectively.

We also evaluated the impact of fumaric acid on the disproportionation of the HCl salt, where disproportionation was significantly more severe due to its inherent instability. Fumaric acid was found to be equally effective in the HCl salt mixture. Figure 15(b) shows that the HCl salt breaks down completely at 12.5 mg/mL concentration. However, the addition of fumaric acid allowed the mixture to remain freebase-free even after 400 min. Interestingly, it was found that, at the end of the experiment, the mixture contained approximately 30% HCl salt and 70% hemifumarate.

3.5.3. Further Optimization Opportunities. The stress test employed in this study was unconventional. The choice of temperature and concentration ranges afford appropriate property differentiation, allowing the disproportionation transformation to be effectively tracked in a reasonable time frame. While the salt itself and the salt/acid modifier pair are the focus of this investigation, there are other components in the formulation (diluents, fillers, binders, disintegrants, and lubricants), as well as factors such as manufacturing unit operations; both could conceivably lead to unexpected interactions that influence drug product performance. For the amount of fumaric acid in the stress test, we used 5% of the total tablet weight, which translates to an acid/API molar ratio of ~0.73 (0.50 would be the theoretical molar ratio for hemifumarate). Although it was not varied in this study, it is reasonable to assume that the amount of fumaric acid can be further optimized. Our initial choice of 5% fumaric acid in the formulation composition worked well in development. In clinical trials, we were able to consistently meet and exceed the desired efficacy as guided by the Target Product Profile of the drug candidate.

https://doi.org/10.1021/acs.molpharmaceut.4c00166
Mol. Pharmaceutics 2024, 21, 2590−2605

4. CONCLUSIONS

We started by attempting salt formation to address compound X's extreme solubility (intrinsic solubility = 8 μg/mL) challenge. A narrow window of developability was created after a thorough screening covering more than 30 counterions and cocrystal partners afforded two salts (HCl and maleate) and one cocrystal (hemifumarate). The physical stability (dehydration) of the HCl salt was flagged during solid-state evaluation, but it was through the preformulation studies that major risks of the HCl salt, and salts in general, were revealed: pH-dependent solubility and the propensity of salt disproportionation. The relatively low pH_{max} values of the salts are also indicative of the disproportionation activities. The maleate was selected for development due to its balanced stability and solubility profile. To develop the maleate into a feasible product despite disproportionation liability, we resorted to a differentiating stress test, which further confirmed the maleate's superior robustness (vs HCl salt). An improved chemometric model originating from a previous publication[48] and an orthogonal X-ray analysis were utilized for the quantitation and kinetic assessment of the disproportionation event, further enhancing the understanding of the process.

We took a strategic approach to select fumaric acid as the pH modulator to include in the drug product. We had projected hemifumarate's better stability based on insight from crystal structure elucidation. This advantage is leveraged in the maleate-fumaric duo, where fumaric acid regulates the microenvironmental pH and prevents freebase precipitation by combining with it to form the hemifumarate. The stress experiments provided compelling evidence of the benefit of fumaric acid, where the solubility could be effectively maintained at the salt-cocrystal level. In the formulation development framework of spring-and-parachute, our innovative design leads to a spring-parachute-safety-net model (Figure 16) that extends the drug absorption by preventing/delaying the solubility drop to the ground (neutral form) level. We believe that this approach has broader application potential in the development of other pharmaceutical products. In situations where pH modulation (acidifier or alkalizer) is required, the modifiers should be comprehensively screened for the possibility of salt and cocrystal formation. Synergistic solubility behavior, such as the case presented in this work, offers new opportunities beyond conventional formulation to suppress disproportionation.

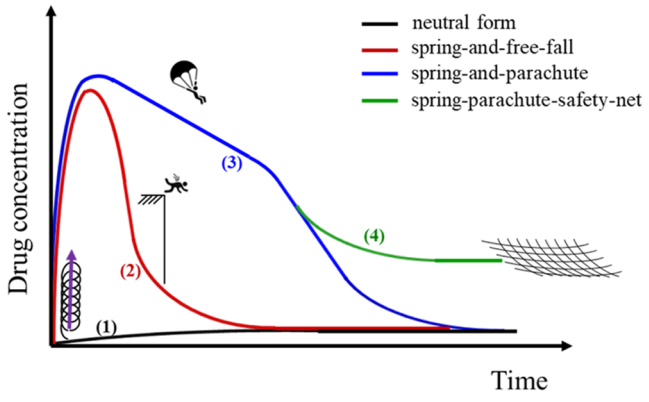

Figure 16. Schematic representations of different drug dissolution and absorption scenarios: (1) slow dissolution kinetics and low solubility of the neutral form (2) peak dissolution and immediate solubility drop due to precipitation of neutral form (spring-free-fall), (3) peak dissolution followed by mediated solubility drop and inhibited precipitation of the neutral form (spring-and-parachute), and (4) peak dissolution followed by mediated solubility drop and diversion to a secondary moderate-solubility form (spring-parachute-safety-net).

AUTHOR INFORMATION

Corresponding Author

Chiajen Lai − *Gilead Sciences, Inc., Foster City, California 94404, United States;* orcid.org/0000-0002-1699-8616; Email: chiajen.lai@gilead.com

Authors

Shikhar Mohan − *Gilead Sciences, Inc., Foster City, California 94404, United States*

Yi Li − *Gilead Sciences, Inc., Foster City, California 94404, United States*

Kevin Chu − *Velexi Corporation, Burlingame, California 94010, United States*

Liliana De La Paz − *Gilead Sciences, Inc., Foster City, California 94404, United States;* Present Address: Jazz Pharmaceuticals, Palo Alto, California 94304, United States

Diana Sperger − *Gilead Sciences, Inc., Foster City, California 94404, United States*

Bing Shi − *Gilead Sciences, Inc., Foster City, California 94404, United States*

Chris Foti − *Gilead Sciences, Inc., Foster City, California 94404, United States*

Victor Rucker − *Gilead Sciences, Inc., Foster City, California 94404, United States*

Complete contact information is available at: https://pubs.acs.org/10.1021/acs.molpharmaceut.4c00166

Notes

The authors declare no competing financial interest.

ACKNOWLEDGMENTS

Support from the Senior Management of Pharmaceutical Development and Manufacturing (PDM) at Gilead Sciences is greatly appreciated. The authors thank Dr. Jared Smit from Curia Global, Inc. for insightful discussions on single-crystal structure.

REFERENCES

(1) Merisko-Liversidge, E.; Liversidge, G.; Cooper, E. Nanosizing: a formulation approach for poorly-water-soluble compounds. *Eur. J. Pharm. Sci.* **2003**, *18*, 113−120.

(2) Kalepu, S.; Nekkanti, V. Insoluble drug delivery strategies: review of recent advances and business prospects. *Acta Pharm. Sin. B* **2015**, *5*, 442−453.

(3) Kawabata, Y.; Wada, K.; Nakatani, M.; Yamada, S.; Onoue, S. Formulation design for poorly water-soluble drugs based on biopharmaceutics classification system: Basic approaches and practical applications. *Int. J. Pharm.* **2011**, *420*, 1−10.

(4) Verma, V.; Ryan, K. M.; Padrela, L. Production and isolation of pharmaceutical drug nanoparticles. *Int. J. Pharm.* **2021**, *603*, No. 120708.

(5) Loftsson, T.; Duchene, D. Cyclodextrins and their pharmaceutical applications. *Int. J. Pharm.* **2007**, *329*, 1−11.

(6) He, Y.; Ho, C. Amorphous solid dispersions: utilization and challenges in drug discovery and development. *J. Pharm. Sci.* **2015**, *104* (10), 3237−3258.

(7) Schittny, A.; Huwyler, J.; Puchkov, M. Mechanisms of increased bioavailability through amorphous solid dispersions: a review. *Drug Delivery* **2020**, *27* (1), 110−127.
(8) *Regulatory Classification of Pharmaceutical Co-Crystals: Guidance for Industry*; FDA: 2018.
(9) Karimi-Jafari, M.; Padrela, L.; Walker, G. M.; Croker, D. M. Creating Cocrystals: A Review of Pharmaceutical Cocrystal Preparation Routes and Applications. *Cryst. Growth Des.* **2018**, *18*, 6370−6387.
(10) Nie, H.; Byrn, S. R.; Zhou, Q. Stability of pharmaceutical salts in solid dosage forms. *Drug Dev. Ind. Pharm.* **2017**, *43* (8), 1215−1228.
(11) Cruz-Cabeza, A. J. Acid-base crystalline complexes and the pKa rule. *CrystEngComm* **2012**, *14* (20), 6362−6365.
(12) Childs, S.; Stahly, G. P.; Park, A. The salt-crystal continuum: the influence of crystal structure on ionization state. *Mol. Pharm.* **2007**, *4*, 323−338.
(13) Saal, C.; Becker, A. Pharmaceutical Salts: A Summary on Doses of Salt Formers from the Orange Book. *Eur. J. Pharm. Sci.* **2013**, *49* (4), 614−623.
(14) Stahl, P. H.; Wermuth, C. G. *Handbook of Pharmaceutical Salts: Properties, Selection, and Use*; Wiley-VCH, 2008.
(15) Guerrieri, P.; Taylor, L. S. Role of Salt and Excipient Properties on Disproportionation in the Solid-State. *Pharm. Res.* **2009**, *26* (8), 2015−2026.
(16) Stephenson, G. A.; Aburub, A.; Woods, T. A. Physical stability of salts of weak bases in the solid-state. *J. Pharm. Sci.* **2011**, *100*, 1607−1617.
(17) Hsieh, Y.-L.; Taylor, L. S. Salt Stability - Effect of Particle Size, Relative Humidity, Temperature and Composition on Salt to Free Base Conversion. *Pharm. Res.* **2015**, *32*, 549−561.
(18) Thakral, N. K.; Kelly, R. C. Salt disproportionation: A material science perspective. *Int. J. Pharm.* **2017**, *520*, 228−240.
(19) Koranne, S.; Lalge, R.; Suryanarayanan, R. Modulation of Microenvironmental Acidity: A Strategy to Mitigate Salt Disproportionation in Drug Product Environment. *Mol. Pharm.* **2020**, *17*, 1324−1334.
(20) Merritt, J. M.; Viswanath, S. K.; Stephenson, G. A. Implementing Quality by Design in Pharmaceutical Salt Selection: A Modeling Approach to Understanding Disproportionation. *Pharm. Res.* **2012**, *30*, 203−217.
(21) Weldeab, A. O.; McElderry, J.; Lin, Y. The Effect of In-Situ-Generated Moisture on Disproportionation of Pharmaceutical Salt. *Mol. Pharm.* **2023**, *20*, 561−571.
(22) Serajuddin, A. T. M. Salt formation to improve drug solubility. *Adv. Drug Delivery Rev.* **2007**, *59*, 603−616.
(23) Christensen, N. P. A.; Rantanen, J.; Cornett, C.; Taylor, L. S. Disproportionation of the calcium salt of atorvastatin in the presence of acidic excipients. *Eur. J. Pharm. Biopharm.* **2012**, *82*, 410−416.
(24) Hsieh, Y.-L.; Merritt, J. M.; Yu, W.; Taylor, L. S. Salt Stability − The Effect of pH_{max} on Salt to Freebase Conversion. *Pharm. Res.* **2015**, *32*, 3110−3118.
(25) Patel, M. A.; Luthra, S.; Shamblin, S. L.; Arora, K. K.; Krzyzaniak, J. F.; Taylor, L. S. Effect of excipient properties, water activity, and water content on the disproportionation of a pharmaceutical salt. *Int. J. Pharm.* **2018**, *546*, 226−234.
(26) Abouselo, A.; Rance, G. A.; Tres, F.; Taylor, L. S.; Kwokal, A.; Renou, L.; Scurr, D. J.; Burley, J. C.; Aylott, J. W. Effect of Excipients on Salt Disproportionation during Dissolution: A Novel Application of In-Situ Raman Imaging. *Mol. Pharm.* **2021**, *18*, 3247−3259.
(27) Nie, H.; Xu, W.; Taylor, L. S.; Marsac, P. J.; Byrn, S. R. Crystalline solid dispersion-a strategy to slowdown salt disproportionation in solid state formulations during storage and wet granulation. *Int. J. Pharm.* **2017**, *517*, 203−215.
(28) Park, J.-B.; Park, Y.-J.; Kang, C.-Y.; Lee, B.-J. Modulation of microenvironmental pH and utilization of alkalizers in crystalline solid dispersion for enhanced solubility and stability of clarithromycin. *Arch. Pharmacal Res.* **2015**, *38*, 839−848.
(29) Van Nguyen, H.; Baek, N.; Lee, B.-J. Enhanced gastric stability of esomeprazole by molecular interaction and modulation of microenvironmental pH with alkalizers in solid dispersion. *Int. J. Pharm.* **2017**, *523*, 189−202.
(30) Hou, H. H.; Jia, W.; Liu, L.; Cheeti, S.; Li, J.; Nauka, E.; Nagapudi, K. Effect of Microenvironmental pH Modulation on the Dissolution Rate and Oral Absorption of the Salt of a Weak Acid − Case Study of GDC-0810. *Pharm. Res.* **2018**, *35*, No. 37.
(31) Ploen, J.; Andersch, J.; Heschel, M.; Leopold, C. S. Citric acid as a pH-modifying additive in an extended-release pellet formulation containing a weakly basic drug. *Drug Dev. Ind. Pharm.* **2009**, *35* (10), 1210−1218.
(32) Bassi, P.; Kaur, G. pH modulation: a mechanism to obtain pH-independent drug release. *Expert Opin. Drug Delivery* **2010**, *7* (7), 845−857.
(33) Taniguchi, C.; Kawabata, Y.; Wada, K.; Yamada, S.; Onoue, S. Microenvironmental pH-modification to improve dissolution behavior and oral absorption for drugs with pH-dependent solubility. *Expert Opin. Drug Delivery* **2014**, *11* (4), 505−516.
(34) Tran, P. H.-L.; Tran, T. T.-D.; Lee, K.-H.; Kim, D.-J.; Lee, B.-J. Dissolution modulating mechanism of pH modifiers in solid dispersion containing weakly acidic or basic drugs with poor water solubility. *Expert Opin. Drug Delivery* **2010**, *7* (5), 647−661.
(35) Wairkar, S.; Gaud, R.; Jadhav, N. Enhanced dissolution and bioavailability of Nateglinide by microenvironmental pH-regulated ternary solid dispersion: in-vitro and in-vivo evaluation. *J. Pharm. Pharmacol.* **2017**, *69*, 1099−1109.
(36) Vo, A. Q.; Feng, X.; Zhang, J.; Zhang, F.; Repka, M. A. Dual mechanism of microenvironmental pH modulation and foam melt extrusion to enhance performance of HPMCAS based amorphous solid dispersion. *Int. J. Pharm.* **2018**, *550*, 216−228.
(37) Siepe, S.; Lueckel, B.; Kramer, A.; Ries, A.; Gurny, R. Strategies for the design of hydrophilic matrix tablets with controlled microenvironmental pH. *Int. J. Pharm.* **2006**, *316*, 14−20.
(38) Badawy, S. I. F.; Hussain, M. A. Microenvironmental pH Modulation in Solid Dosage Forms. *J. Pharm. Sci.* **2007**, *96*, 948−959.
(39) Cristofoletti, R.; Dressman, J. B. Dissolution methods to increasing discriminatory power of in vitro dissolution testing for ibuprofen free acid and its salts. *J. Pharm. Sci.* **2017**, *106*, 92−99.
(40) Krieg, B. J.; Taghavi, S. M.; Amidon, G. L.; Amidon, G. E. In vivo predictive dissolution: comparing the effect of bicarbonate and phosphate buffer on the dissolution of weak acids and weak bases. *J. Pharm. Sci.* **2015**, *104*, 2894−2904.
(41) Dokoumetzidis, A.; Macheras, A. A century of dissolution research: from Noyes and Whitney to the biopharmaceutics classification system. *Int. J. Pharm.* **2006**, *321*, 1−11.
(42) Haznar-Garbacz, D.; Hoc, D.; Garbacz, G.; Lachman, M.; Slominska, D.; Romanski, M. Dissolution of a Biopharmaceutical Classification System Class II Free Acid from Immediate Release Tablets Containing a Microenvironmental pH Modulator: Comparison of a Biorelevant Bicarbonate Buffering System with Phosphate Buffers. *AAPS PharmSciTech* **2022**, *23*, 203.
(43) Tran, P. H. L.; Tran, H. T. T.; Lee, B.-J. Modulation of microenvironmental pH and crystallinity of ionizable telmisartan using alkalizers in solid dispersions for controlled release. *J. Controlled Release* **2008**, *129*, 59−65.
(44) Bavishi, D. D.; Borkhataria, C. H. Spring and parachute: How cocrystals enhance solubility. *Prog. Cryst. Growth Charact. Mater.* **2016**, *62*, 1−8.
(45) Liu, C.; Chen, Z.; Chen, Y.; Lu, J.; Li, Y.; Wang, S.; Wu, G.; Qian, F. Improving Oral Bioavailability of Sorafenib by Optimizing the "Spring" and "Parachute" Based on Molecular Interaction Mechanisms. *Mol. Pharm.* **2016**, *13*, 599−608.
(46) Guo, X.; Guo, Y.; Zhang, M.; Yang, B.; Liu, H.; Yin, T.; Zhang, Y.; He, H.; Wang, Y.; Liu, D.; Gou, J.; Tang, X. A comparative study on in vitro and in vivo characteristics of enzalutamide nanocrystals versus amorphous solid dispersions and a better prediction for bioavailability based on "spring-parachute" model. *Int. J. Pharm.* **2022**, *628*, No. 122333.

https://doi.org/10.1021/acs.molpharmaceut.4c00166
Mol. Pharmaceutics 2024, 21, 2590−2605

(47) Morrison, H.; Fung, P.; Horstman, E.; Lapina, O.; Khuth, T.; Lye, D. S.; Regens, C. S.; Bringley, D.; Alleva, J. Application of Twin Screw Extrusion to Scale Polymorphs, a Salt, and the Amorphous Phase for Various Drug Substances. *Org. Process Res. Dev.* **2024**, *28*, 1186−1194.
(48) Mohan, S.; Li, Y.; Chu, K.; Shi, B.; De La Paz, L.; Bakre, P.; Foti, C.; Rucker, V.; Lai, C. Developing In Situ Chemometric Models with Raman Spectroscopy for Monitoring an API Disproportionation with a Complex Polymorphic Landscape. *Pharmaceuticals* **2023**, *16* (2), No. 327.
(49) Popović, S. Quantitative phase analysis by X-ray diffraction − doping methods and applications. *Crystals* **2020**, *10* (1), No. 27.
(50) US Pharmacopeia (USP) stage 4 harmonization, USP, Characterization of crystalline and partially crystalline solids by X-ray powder diffraction 2022.
(51) Fung, P.; Mah, H.; Goldberg, A.; Rieder, C.; Sun, H.-Y.; Su, J.; Du, J.; Lai, C. PAT-Facilitated Pharmaceutical Crystallization Development through Mechanistic Understanding. *Cryst. Growth Des.* **2020**, *20*, 7882−7900.
(52) Cardew, P. T. Ostwald Rule of Stages - Myth or Reality. *Cryst. Growth Des.* **2023**, *23* (6), 3958−3969.
(53) Cavanagh, K. L.; Maheshwari, C.; Rodriguez-Hornedo, N. Understanding the Differences Between Cocrystal and Salt Aqueous Solubilities. *J. Pharm. Sci.* **2018**, *107*, 113−120.
(54) Tran, T. T.-D.; Tran, P. H.-L.; Choi, H.-G.; Han, H.-K.; Lee, B.-J. The roles of acidifiers in solid dispersions and physical mixtures. *Int. J. Pharm.* **2010**, *384*, 60−66.
(55) Rowe, R. C.; Sheskey, P. J.; Quinn, M. E. *Handbook of Pharmaceutical Excipients*, 6th ed.; Pharmaceutical Press, 2009.

https://doi.org/10.1021/acs.molpharmaceut.4c00166
Mol. Pharmaceutics 2024, 21, 2590−2605